Degradation of unmethylated miRNA/miRNA*s by a DEDDy-type 3′ to 5′ exoribonuclease Atrimmer 2 in *Arabidopsis*

Xiaoyan Wang[a,b,c,1], Yuan Wang[a,b,1], Yongchao Dou[d,e,1], Lu Chen[a,b], Junli Wang[a,b], Ning Jiang[a,b], Chunce Guo[a,b], Qingqing Yao[a,b], Chizao Wang[a,b], Lin Liu[c], Bin Yu[f], Binglian Zheng[a,b], Julia A. Chekanova[g,2], Jinbiao Ma[a,b], and Guodong Ren[a,b,3]

[a]State Key Laboratory of Genetic Engineering, School of Life Sciences, Fudan University, 200438 Shanghai, China; [b]Institute of Plant Biology, School of Life Sciences, Fudan University, 200438 Shanghai, China; [c]Guangdong Province Key Laboratory for Plant Epigenetics, College of Life Science and Oceanography, Shenzhen University, 518060 Shenzhen, China; [d]Lester and Sue Smith Breast Center, Baylor College of Medicine, Houston, TX 77030; [e]Department of Molecular and Human Genetics, Baylor College of Medicine, Houston, TX 77030; [f]Center for Plant Science Innovation and School of Biological Sciences, University of Nebraska-Lincoln, Lincoln, NE 68588-0660; and [g]School of Biological Sciences, University of Missouri-Kansas City, Kansas City, MO 64110

Edited by Natasha V. Raikhel, Center for Plant Cell Biology, Riverside, CA, and approved May 31, 2018 (received for review December 16, 2017)

The 3′ end methylation catalyzed by HUA Enhancer 1 (HEN1) is a crucial step of small RNA stabilization in plants, yet how unmethylated small RNAs undergo degradation remains largely unknown. Using a reverse genetic approach, we here show that Atrimmer 2 (ATRM2), a DEDDy-type 3′ to 5′ exoribonuclease, acts in the degradation of unmethylated miRNAs and miRNA*s in *Arabidopsis*. Loss-of-function mutations in ATRM2 partially suppress the morphological defects caused by HEN1 malfunction, with restored levels of a subset of miRNAs and receded expression of corresponding miRNA targets. Dysfunction of ATRM2 has negligible effect on miRNA trimming, and further increase the fertility of *hen1 heso1 urt1*, a mutant with an almost complete abolishment of miRNA uridylation, indicating that ATRM2 may neither be involved in 3′ to 5′ trimming nor be the enzyme that specifically degrades uridylated miRNAs. Notably, the fold changes of miRNAs and their corresponding miRNA*s were significantly correlated in *hen1 atrm2* versus *hen1*. Unexpectedly, we observed a marked increase of 3′ to 5′ trimming of several miRNA*s but not miRNAs in ATRM2 compromised backgrounds. These data suggest an action of ATRM2 on miRNA/miRNA* duplexes, and the existence of an unknown exoribonuclease for specific trimming of miRNA*. This asymmetric effect on miRNA/miRNA* is likely related to Argonaute (AGO) proteins, which can distinguish miRNAs from miRNA*s. Finally, we show that ATRM2 colocalizes and physically interacts with Argonaute 1 (AGO1). Taken together, our results suggest that ATRM2 may be involved in the surveillance of unmethylated miRNA/miRNA* duplexes during the initiation step of RNA-induced silencing complex assembly.

ATRM2 | miRNA | degradation | exoribonuclease | methylation

MicroRNAs (miRNAs) are a class of endogenous small noncoding RNAs with 20–24 nucleotides (nt) in size. They play important roles in reproduction, development, and responses to environmental stimuli by negatively regulating gene expression through target RNA cleavage, deadenylation-mediated RNA decay, and/or translation inhibition (1). The transcription, processing, and stability of miRNAs are spatiotemporally controlled to ensure their optimal cellular levels. In plants, miRNAs are transcribed by RNA Polymerase II (Pol II) and processed into miRNA/miRNA* duplex by an RNase III endoribonuclease Dicer-like 1 (DCL1) (2, 3). The 3′ terminal ribose on each strand of the miRNA/miRNA* duplex is methylated by the small RNA methyltransferase HUA Enhancer 1 (HEN1), before being channeled onto Argonaute 1 (AGO1) to form the miRNA-induced silencing complex (miRISC) (4). The 5′ terminal nucleotide, duplex structure, and asymmetric thermostability of miRNA/miRNA* duplex are important for Argonaute sorting and/or guide strand selection (reviewed in refs. 5–7). In plants, loss of function in the dsRNA binding protein Hyponastic Leaves 1 (HYL1) not only diminishes the production of miRNAs (i.e., guide strands), but also increases the abundance of some miRNA*s (i.e., passenger strands), suggesting that HYL1 may also be involved in miRNA strand selection, which bridges the gap between miRNA biogenesis and RISC assembly (8).

HEN1-mediated 3′ end methylation is crucial for the stability of miRNAs in plants and piRNAs in animals (9). In the absence of HEN1, miRNAs undergo extensive 3′ tailing (predominantly uridylation) and 3′ to 5′ trimming (4, 10). Two terminal uridylyl transferases, HEN1 Suppressor 1 (HESO1) and UTP:RNA Uridylyltransferase 1 (URT1), act synergistically to add one to six uridines to the 3′ termini of miRNAs, which triggers their degradation by yet unknown enzymes (11–14). Unlike methylation, miRNA tailing likely occurs after RISC loading (15, 16). The 3′ to 5′ trimming seems to antagonize with tailing because loss of tailing in the *hen1 heso1 urt1* mutant is accompanied by an extensive

Significance

The steady-state levels of miRNAs are under sophisticated control to ensure their proper functions such as development and responses to environmental stimuli. Nevertheless, enzymes responsible for the degradation of various forms of unmethylated miRNAs remain enigmatic, which largely impedes our understanding of miRNA homeostasis and active turnover. Here we report a 3′ to 5′ exoribonuclease Atrimmer 2 that may degrade unmethylated miRNAs in their miRNA/miRNA* duplex status, at places distinct from their production sites (i.e., Dicing bodies). Our study not only increases the complexity of miRNA surveillance, but also provides clues into how nascent miRNA/miRNA* duplexes undergo methylation and RNA-induced silencing complex loading, which is a big challenge in the plant small RNA field.

Author contributions: X.W. and G.R. designed research; X.W., Y.W., L.C., J.W., Q.Y., C.W., and L.L. performed research; B.Y., B.Z., J.A.C., and J.M. contributed new reagents/analytic tools; X.W., Y.D., N.J., C.G., and G.R. analyzed data; and X.W. and G.R. wrote the paper.

The authors declare no conflict of interest.

This article is a PNAS Direct Submission.

Data deposition: The data reported in this paper have been deposited in the Gene Expression Omnibus (GEO) database, https://www.ncbi.nlm.nih.gov/geo (accession no. GSE107070).

[1]X.W., Y.W., and Y.D. contributed equally to this work.

[2]Present address: Mycological Research Center, College of Life Science, Fujian Agriculture and Forestry University, 350002 Fuzhou, China.

[3]To whom correspondence should be addressed. Email: gdren@fudan.edu.cn.

This article contains supporting information online at www.pnas.org/lookup/suppl/doi:10.1073/pnas.1721917115/-/DCSupplemental.

Published online June 25, 2018.

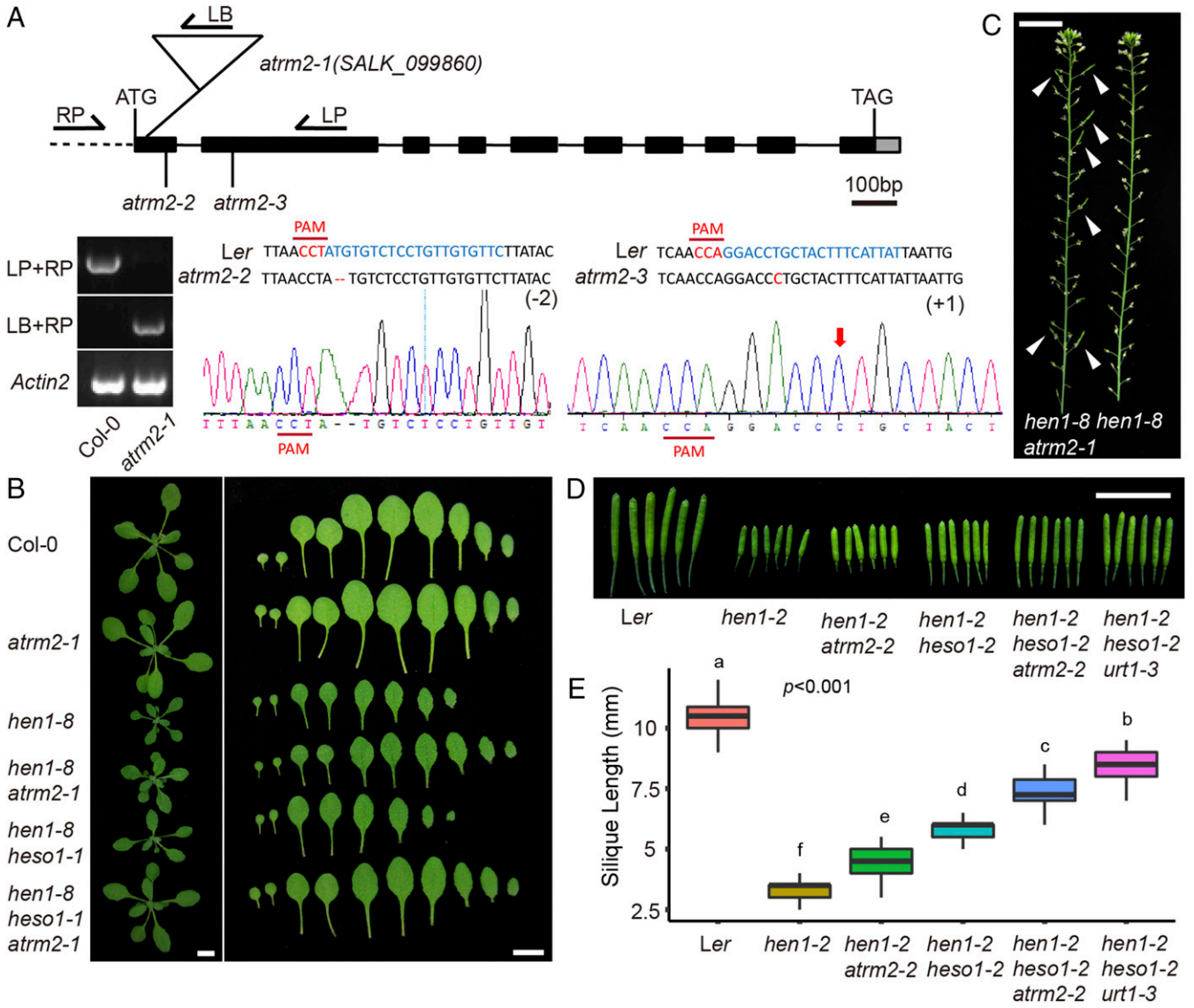

Fig. 1. *ATRM2* mutations partially suppress the morphological defects of *hen1* and *hen1 heso1*. (*A*) *ATRM2* gene structure and various *atrm2* mutants used in this study. LP, RP, and LB, primers used for genotyping of *atrm2-1*; PAM, protospacer adjacent motif. LB, T-DNA left border primer; LP, *ATRM2* left primer; RP, *ATRM2* right primer. (*B*) *atrm2-1* restores the phyllochron of *hen1-8* and *hen1-8 heso1-1*. Three-week-old plants and their rosette leaves are shown. (*C*) *atrm2-1* partially restores the fertility of *hen1-8*. Primary inflorescences of *hen1-8 atrm2* and *hen1-8* from 6-wk old plants are shown. White triangles indicate fertile siliques. (*D*) *atrm2-1* partially restores the fertility of *hen1-2* and *hen1-2 heso1-2*. (*E*) Quantification of silique length in various genotypes. For each genotype, 30~40 siliques from at least six individual plants were analyzed. Different letters indicate statistically significant differences (ANOVA test, $P < 0.001$). (Scale bar: 1 cm.)

increase in trimming (11). Nevertheless, the enzyme that catalyzes the trimming reaction of unmethylated miRNAs has not yet been identified, and as such, the precise effect of trimming modification on miRNA stability remains unclear. In addition, the enzyme(s) directly involved in the degradation of unmethylated miRNAs has not been characterized.

The 3′ to 5′ exoribonucleases are evolutionarily conserved enzymes that play diverse roles in almost all aspects of RNA metabolic processes. Five superfamilies of 3′ to 5′ exoribonucleases, namely DEDD, PDX, RNR, RBN, and RRP4, have been classified based on sequence conservation (17). The DEDD superfamily can be further divided into the DEDDh and DEDDy subfamilies according to the distinct conservation patterns in motif III {i.e., H-x[4]-D for DEDDh and Y-x[3]-D for DEDDy} (17). In animals, a number of 3′ to 5′ exoribonucleases are involved in diverse steps of different RNAi pathways (18–21). Most of them belong to the DEDDh subfamilies except for MUT-7 in *Caenorhabditis elegans* and Nibbler in *Drosophila*, which are the DEDDy subfamily exoribonucleases. MUT-7 interacts with another RNAi factor RDE-2 and acts possibly in the step of siRNA amplification (22). Nibbler was originally identified to trim the 3′ ends of a subset of 24 nt miRNAs on AGO1 into isoforms with the preferred length (19, 20). Recently, Nibbler was reported to resect a subset of prepiRNAs to mature piRNAs, representing a novel piRNA 3′ end formation pathway that parallels the Zucchini pathway (23).

In *Arabidopsis*, Small RNA Degrading Nucleases (SDNs), a class of DEDDh 3′ to 5′ end exoribonucleases, are involved in plant miRNA decay (24). Since SDNs can degrade methylated miRNAs, SDNs may serve as a "demethylase" by trimming off the last few nucleotides (25). Importantly, a small fraction of miRNAs in wild-type (WT) plants is also unmethylated and can be uridylated and/or trimmed, with patterns similar to those in *hen1* (11). It has been postulated that uridylation and trimming may play a role in miRNA surveillance and quality control or act

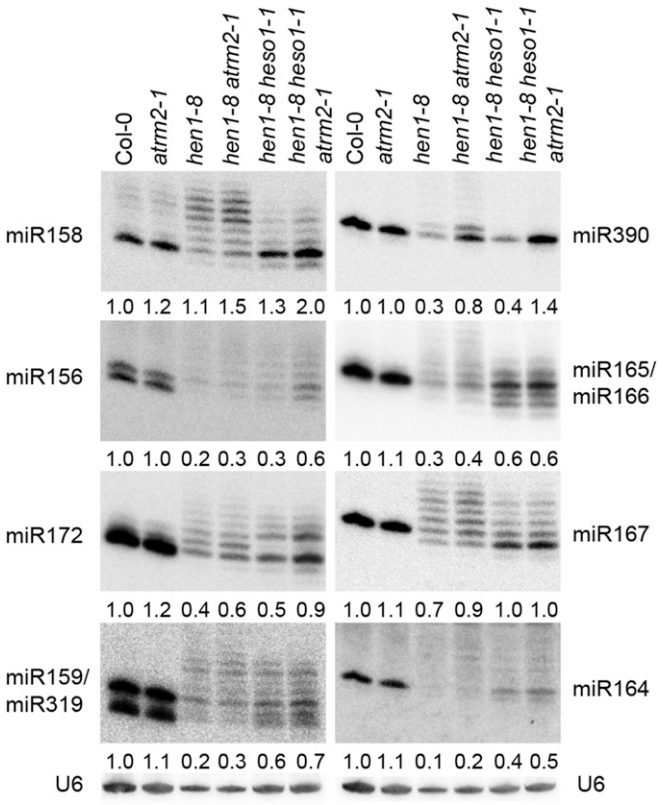

Fig. 2. Comparison of miRNA expression and profiles among different genotypes by small RNA Northern blots (long gel). Low molecular weight (LMW) RNA extracted from inflorescence tissues of indicated genotype was used. U6 was used as a loading control.

downstream of SDNs during active turnover (26). Although a DEDDy exoribonuclease WEX has been shown to be involved in sense transgene-induced posttranscriptional gene silencing (S-PTGS), its function remains elusive (27).

In the course of seeking enzymes that are responsible for either 3′ to 5′ trimming or degradation of unmethylated miRNAs in *Arabidopsis*, we discovered that loss of function in ATRM2, a DEDDy type 3′ to 5′ exoribonuclease, rescues the *hen1* phenotype by selectively increasing the abundance of a subset of miRNAs, without affecting the trimming and tailing profiles. Further genetic analysis indicates that ATRM2 functions downstream of methylation but possibly upstream of uridylation. Notably, we found a significant coregulation of miRNAs and their corresponding miRNA*s by ATRM2. For at least some miRNA*s, we found an overaccumulation of trimmed species by loss of ATRM2, a pattern not observed for miRNAs, suggesting the involvement of AGO selection. These data, together with the result that ATRM2 colocalizes and physically interacts with AGO1, indicate that ATRM2 may function in miRNA quality control by unmethylated miRNA/miRNA* duplex surveillance during the initiation step of RISC loading.

Results

Loss of ATRM2 Function Partially Suppresses the Morphological Defects of *hen1* and *hen1 heso1*. To identify genes that are responsible for either 3′ to 5′ trimming or degradation of unmethylated miRNAs, protein sequences of 32 known 3′ to 5′ exoribonucleases (Dataset S1), representing the RNR, DEDDy/h, RBN, PDX, and RRP4 exoribonuclease superfamilies, were used to BLAST against the *Arabidopsis* protein database (www.arabidopsis.org; TAIR v10.0). A total of 64 genes were retrieved with a cutoff e-value of 10E-6 (Dataset S1). In this manuscript, we focused on the DEDDy subfamily exoribonucleases, as several members of this subfamily have been reported to be involved in RNA silencing. Among 13 DEDDy proteins retrieved, 3 were targeted to chloroplast/mitochondria and 5 showed variations in core residues (i.e., DEDDy). These proteins were excluded from further analysis except EXD1, which had conserved DEDD but bore a Y to A substitution (*SI Appendix*, Fig. S1 *A* and *C*). For the remainder, we ordered T-DNA insertion mutants from the *Arabidopsis* Biological Resource Center (ABRC) and crossed each of them into *hen1-8 heso1-1*, which contained a weak allele of HEN1 and a null allele of HESO1, and is in the same ecotype (Columbia, Col-0) as T-DNA mutants (13). We assumed that disruptions of the enzyme(s) involved in trimming or decay of miRNAs would either enhance or suppress the phenotype of plants carrying mutations in *HEN1*. We used *hen1-8 heso1-1* instead of *hen1-8* simply because we were able to obtain a different combination of mutants in one cross experiment, which facilitated our follow-up analyses.

One T-DNA insertion mutant (*SALK_099860*) disrupting At1G56310, but not other tested ones, greatly rescued the morphological defects of *hen1-8* and *hen1-8 heso1-1*, including accelerated growth, better fertility, and recovered phyllochron (Fig. 1 *A*–*C* and *SI Appendix*, Fig. S2 *A* and *B*). At1G56310 was previously shown to be involved in sidRNA (for siRNA independent of DCLs) biogenesis through 3′ to 5′ trimming of AGO4 bound sidRNA precursors and was named *Atrimmer 2* (28) (*ATRM2*, *SALK_099860* accordingly called *atrm2-1*). Nevertheless, our following miRNA profiling suggests that it may not be involved in 3′ to 5′ trimming of miRNAs (Figs. 2 and 3*D* and *SI Appendix*, Fig. S9*A*). According to our phylogenetic analysis, At5g24340 shares the highest homology with ATRM2 and is tentatively named *ATRM2-Like* (*ATRM2L*) (*SI Appendix*, Fig. S1*A*). To test whether ATRM2L acts redundantly with ATRM2, we introduced *atrm2l* into *hen1-8 atrm2-1* and *hen1-8 heso1-1 atrm2-1*, respectively. We found that *hen1-8 atrm2-1 atrm2l-1* and *hen1-8 heso1-1 atrm2-1 atrm2l-1* was morphologically indistinguishable from *hen1-8 atrm2-1* and *hen1-8 heso1-1 atrm2-1*, respectively (*SI Appendix*, Fig. S2*C*), arguing against the role of ATRM2L in miRNA decay pathway.

To validate the role of ATRM2 as a *hen1* suppressor, we transformed a genomic fragment of *ATRM2* fused with a GFP at its C terminus (*pATRM2::ATRM2-GFP*) into *hen1-8 heso1-1 atrm2-1* and found it fully restored the fertility and phyllochron to the *hen1-8 heso1-1* level (*SI Appendix*, Fig. S3). However, a mutant version of ATRM2 with the key catalytic residues DEDD changed to AADD (ATRM2m2) failed to complement the *hen1-8 heso1-1 atrm2-1* phenotype (*SI Appendix*, Fig. S3*B*). We also knocked out *ATRM2* (*atrm2-2*) in *hen1-2 heso1-2*, which is in the Landsberg *erecta* (L*er*) background (12), using the CRISPR-Cas9 genome editing technique (Fig. 1*A*) (29). As expected, *hen1-2 atrm2-2* and *hen1-2 heso1-2 atrm2-2* produced longer siliques compared with *hen1-2* and *hen1-2 heso1-2*, respectively (Fig. 1 *D* and *E*). Taken together, these results demonstrate that loss of function in ATRM2 was responsible for the phenotypic rescue of *hen1-8 heso1-1*. Under normal growth conditions, both morphology and small RNAs in *atrm2-1* were indistinguishable from those in wild-type plants (Figs. 1*B* and 2), implying that ATRM2 functions downstream of HEN1 and targets unmethylated small RNAs. Indeed, loss of ATRM2 was unable to rescue *hyl1-2* or *se-1*, two miRNA biogenesis pathway mutants (*SI Appendix*, Fig. S4).

Loss of ATRM2 in *hen1* Results in an Increased Level of a Subset of miRNAs with Trimming and Uridylation Largely Unaffected. We next investigated whether loss of ATRM2 activity affected 3′ to 5′ trimming and/or overall amount of miRNAs. The miRNA expression patterns in Col-0 (WT), *atrm2-1*, *hen1-8*, *hen1-8 atrm2-1*, *hen1-8 heso1-1*, and *hen1-8 heso1-1 atrm2-1* were compared by

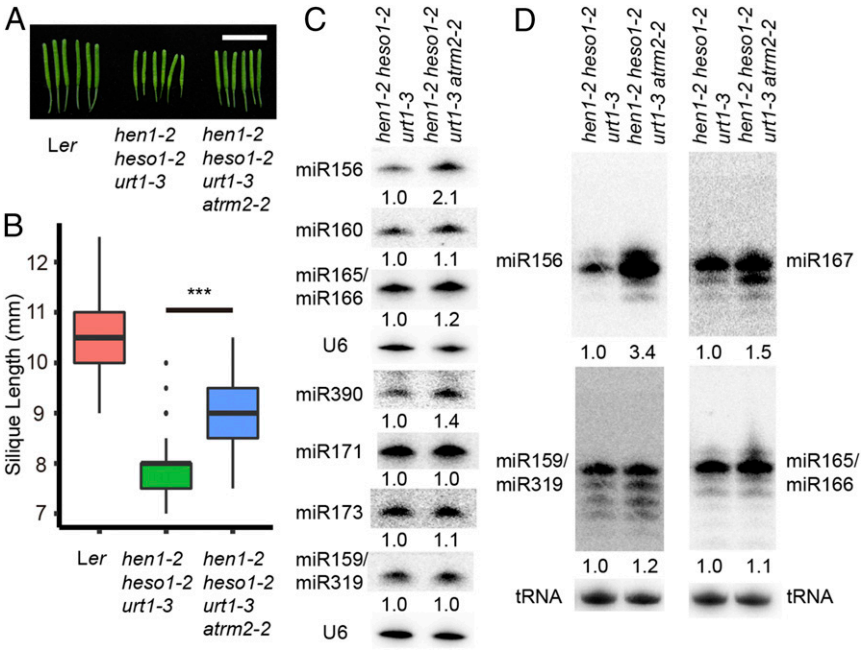

Fig. 3. *atrm2* increases the fertility and the amount of a subset of miRNAs of *hen1-2 heso1-2 urt1-3*. (*A*) Siliques from plants of the indicated genotypes. (Scale bar: 1 cm.) (*B*) Quantification of silique length. For each genotype, 30 siliques from at least six individual plants were analyzed. ***$P < 0.001$, unpaired *t* test. (*C* and *D*) Comparison of miRNA quantity and profiles between *hen1-2 heso1-2 urt1-3* and *hen1-2 heso1-2 urt1-3 atrm2-2* by Northern blots (*C*, short gel; *D*, long gel). LMW RNA extracted from 7-d-old seedlings of indicated genotype was used. U6 (*C*) or tRNA (*D*) was used as a loading control. (Scale bar: 1 cm.)

small RNA Northern blot (Fig. 2). Consistent with our previous report, loss of function in HESO1 significantly shortened miRNA tailing in *hen1* background (12). Strikingly, miRNA profiles in *hen1-8 heso1-1 atrm2-1* resemble those in *hen1-8 heso1-1* for all tested miRNAs (Fig. 2). Similar results were also observed in a parallel set of mutants in the L*er* background (*SI Appendix*, Fig. S5*A*). Notably, the overall abundance of miR156, miR158, miR172, and miR390, but not miR159/319, miR164, miR165/166, miR167, and miR173, were increased by the *ATRM2* mutation, and tended to be more prominent when HESO1 is also compromised (Fig. 2 and *SI Appendix*, Fig. S5*A*). The more accumulation of miR156 and miR390 is consistent with the restored phyllochron and adult-to-juvenile recovery of the first two pairs of true leaves in *hen1-8 heso1-1 atrm2-1* (30–32) (Fig. 1*B* and *SI Appendix*, Fig. S3 *B–D*). Moreover, the miRNA levels were largely unaffected by the *ATRM2L* mutation (*SI Appendix*, Fig. S5*B*), further demonstrating that ATRM2, but not ATRM2L, is involved in miRNA degradation.

Residual HEN1 Activity Is Not Necessary for *atrm2*-Mediated Phenotypic Rescue. Given that both *hen1-8* and *hen1-2* are weak alleles, it is possible that *atrm2* rescues the *hen1*$^{-/-}$ phenotype through enhancing miRNA methylation. To test this, we conducted a β-elimination assay to compare the miRNA methylation level between *hen1-8 heso1-1 atrm2-1* and *hen1-8 heso1-1*. Periodate treatment followed by β-elimination results in faster migration of unmethylated but not methylated miRNAs (4). As shown in *SI Appendix*, Fig. S6, methylation levels of miR156, miR158, and miR167 were comparable between *hen1-8 heso1-1 atrm2-1* and *hen1-8 heso1-1*. Interestingly, methylation of miR390 in *hen1-8 heso1-1 atrm2-1* was remarkably increased relative to that in *hen1-8 heso1-1*. miR390 is specifically associated with AGO7 and modulates plant growth through the transacting siRNA pathway, which depends on RNA-dependent RNA polymerase 6 (RDR6) (33). However, our data showed that *atrm2* was able to rescue the *hen1 rdr6* phenotype, reflecting that miR390 contributes only partially, if at all, to the *atrm2*-mediated phenotypic recovery (*SI Appendix*, Fig. S7).

We also mutated ATRM2 (named *atrm2-3*) in *hen1-1 heso1-2* by CRISPR-Cas9 (Fig. 1*A*). *hen1-1* is a null allele of HEN1. We found that *hen1-1 heso1-2 atrm2-3* grew more vigorously and had better fertility than *hen1-1 heso1-2* (*SI Appendix*, Fig. S8 *A–D*). Therefore, *atrm2*-mediated phenotypic recovery does not rely on residual HEN1 activity.

ATRM2 Negatively Regulates miRNA Function in *hen1*. Since plant miRNAs are mainly involved in target RNA silencing through endogenous cleavage (1), we examined the levels of miRNA targets in WT, *hen1-1*, *hen1-1 heso1-2*, and *hen1-1 heso1-2 atrm2-3* by qPCR, with primers spanning their cleavage sites. As expected, the expression levels of all tested targets were increased in *hen1-1* and their levels were greatly receded in *hen1-1 heso1-2* (*SI Appendix*, Fig. S8*E*). *SPL10*, *TAS3*, and *ARF4*, targets of miR156, miR390, and TAS3, respectively, were further reduced in *hen1-1 heso1-2 atrm2-3* relative to those in *hen1-1 heso1-2* (*SI Appendix*, Fig. S8*E*). Notably, the transcripts of HAP2b/2c and AGL16, which were targeted by miR169 and miR824, respectively, also showed an obvious reduction by the *ATRM2* mutation (*SI Appendix*, Fig. S8*E*). In contrast, *CUC1*, *MYB65*, and *SCL6*, which are targets of miR164, miR159, and miR171, respectively, appeared to be unaffected by the *ATRM2* mutation (*SI Appendix*, Fig. S8*E*). These data were consistent with the result that ATRM2 only affects the abundance of a subset of miRNAs in vivo (Fig. 2 and *SI Appendix*, Fig. S5*A*).

Uridylation Is Dispensable for ATRM2 Function. Our previous study has shown that uridylation of miRNAs can stimulate their degradation (9, 12). We surmised that ATRM2 might degrade uridylated miRNAs. To examine this, we crossed *hen1-2 heso1-2 atrm2-2* with *hen1-2 heso1-2 urt1-3*, a mutant with an almost complete depletion of miRNA uridylation (11). We obtained *hen1-2 heso1-2 urt1-3 atrm2-2* in the F2 generation by genotyping.

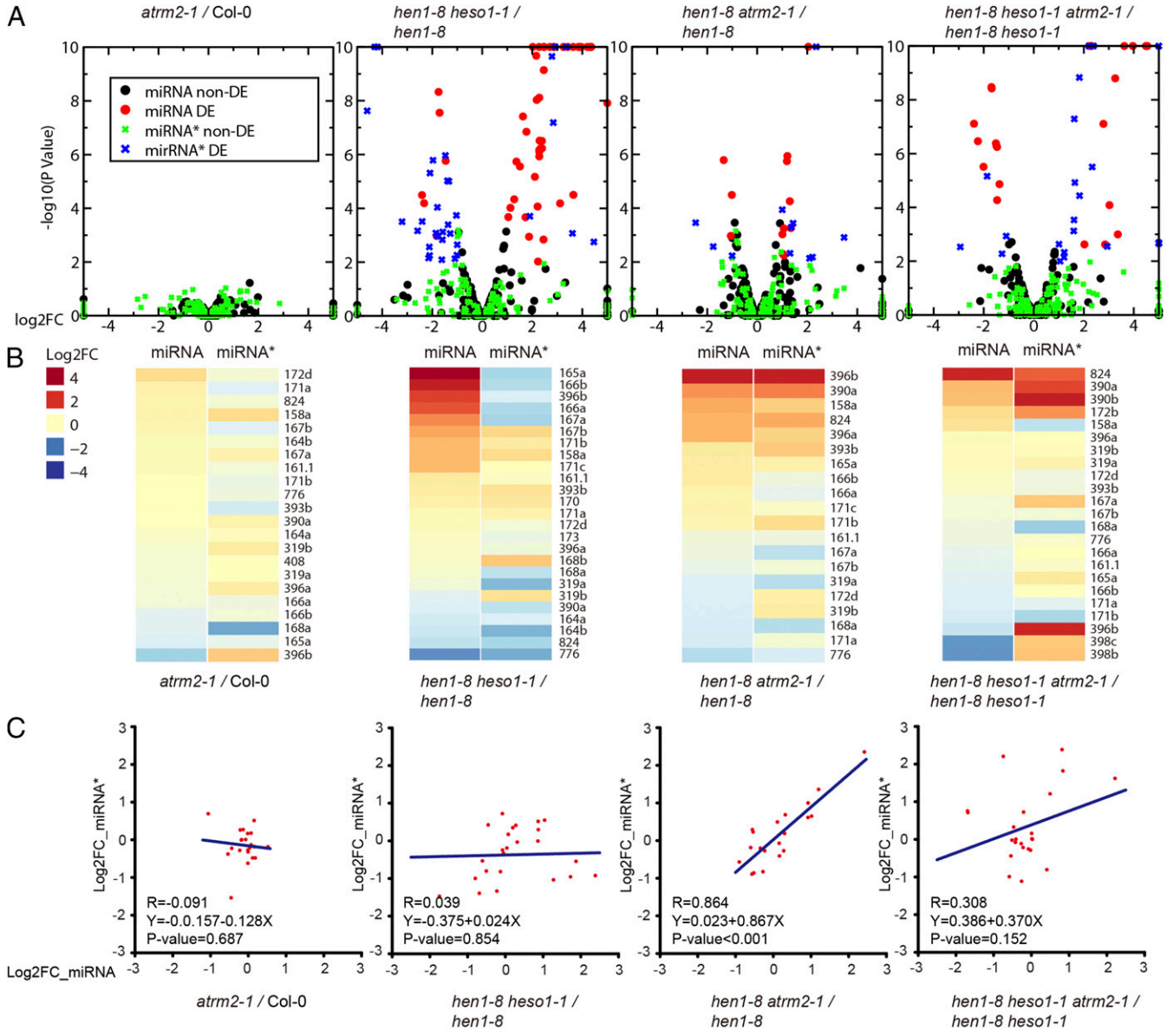

Fig. 4. Coregulation of miRNA and the corresponding miRNA* by ATRM2. (*A*) Differential expressions of miRNAs and miRNAs* shown by volcano plots. DE, differentially expressed; non-DE, nondifferentially expressed. (*B*) Heatmap showing the levels of miRNAs and their corresponding miRNA*s in pairs (ranked by fold change of miRNA). Only high abundant miRNA and miRNA* pairs (with reads per million ≥10) in each library were analyzed. (*C*) Pearson's product moment correlation coefficients among the levels of miRNAs and their corresponding miRNA*s.

We found that the silique length and the abundance of miR156, miR167, and miR390, but not other tested miRNAs, was markedly increased in the *hen1-2 heso1-2 urt1-3 atrm2-2* quadruple mutant compared with those in the *hen1-2 heso1-2 urt1-3* triple mutant (Fig. 3). Although we cannot rule out the possibility that ATRM2 can target and degrade uridylated miRNAs, uridylation seems dispensable for ATRM2 function.

ATRM2 Selectively Degrades a Subset of miRNAs/miRNA*. Considering each band of a miRNA ladder shown by Northern blot might be a mixed effect of trimming and tailing, we therefore performed small RNA deep sequencing to analyze the tailing and trimming patterns quantitatively and globally. Small RNA libraries were constructed from two biological replicates of Col-0, *atrm2-1*, *hen1-8*, *hen1-8 atrm2-1*, *hen1-8 heso1-1*, and *hen1-8 heso1-1 atrm2-1*. Tailing and trimming profiles were analyzed as described previously (11). Loss of ATRM2 in different *hen1* backgrounds resulted in only slightly increased levels of 1 nt trimming or tailing, with the patterns of most examined miRNAs largely unaffected (*SI Appendix*, Fig. S9). Consistent with our Northern blot assay, the abundances of a subset of miRNAs were significantly increased (Fig. 4*A* and Dataset S2). The upregulation of miR824 and miR396 was further validated by Northern blot (*SI Appendix*, Fig. S10). To test whether ATRM2 affects miRNAs and miRNA*s differentially, we reannotated miRNA*s based on miRBase and plant massively parallel signature sequencing (MPSS) database (Dataset S3) (34, 35). Loss of HESO1 globally and predominantly increased the levels of miRNAs, consistent with its role in AGO1-associated miRNAs (Fig. 4*A*). Intriguingly, in addition to miRNAs, many miRNA*s were increased in *hen1 atrm2* and *hen1 heso1 atrm2* relative to their respective controls (Fig. 4*A*). The increase of miRNA*s was validated by Northern blot (Fig. 5*B*). Remarkably, the fold changes of miRNAs and their corresponding miRNA*s were

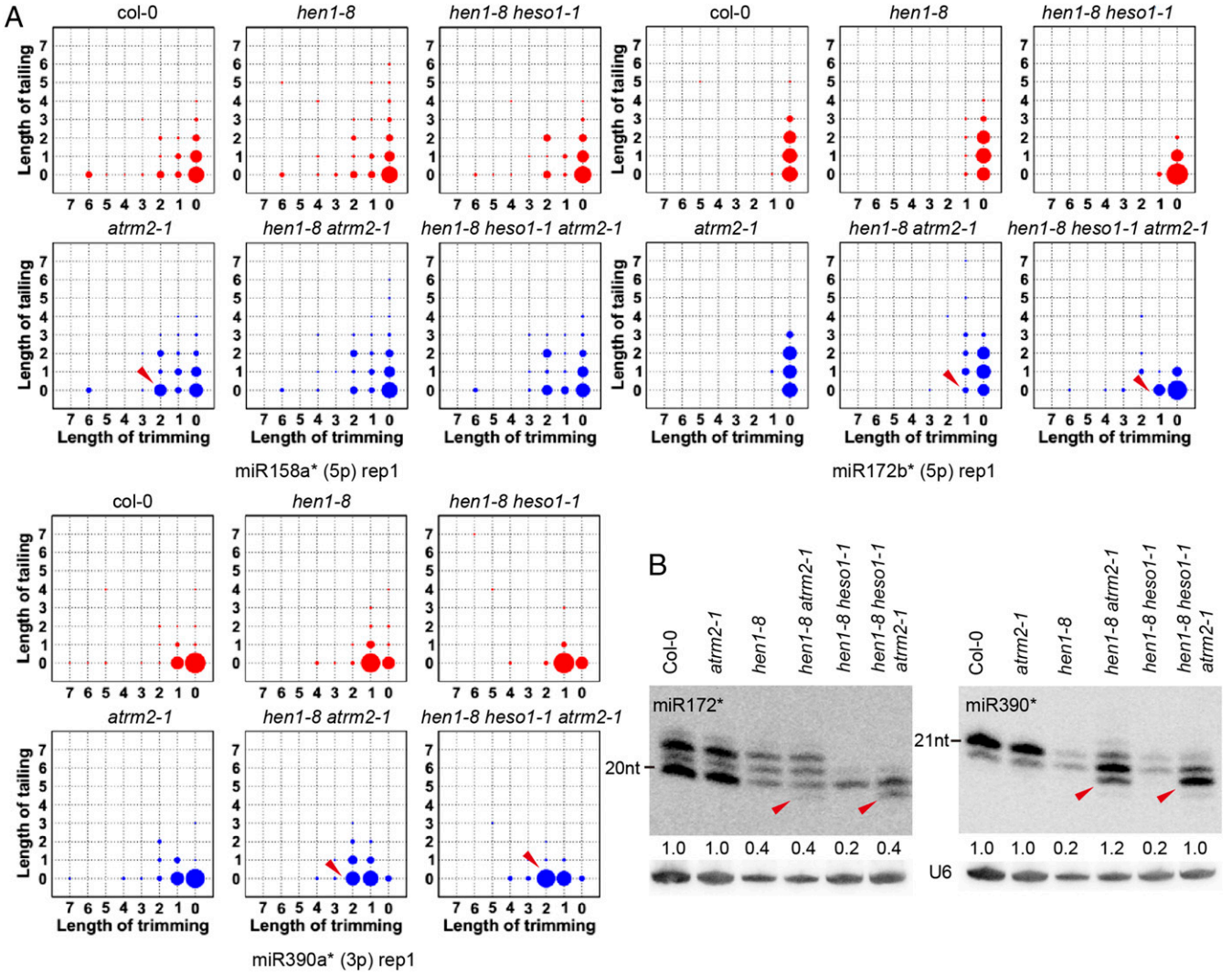

Fig. 5. *atrm2* enhances miRNA* trimming. (*A*) The tailing and trimming profiles of miRNA* from small RNA deep sequencing result. Red arrows indicate major differential miRNA species caused by ATRM2 mutation. The *x* axis represents the degree of trimming and the *y* axis represents the degree of tailing. The reannotated miRNA* sequences (Dataset S3) based on miRBase v21 served as standard sequences. The relative amount of each small RNA species is proportional to the diameter of the circles. See *SI Appendix*, Fig. S11*A* for data from biological replicate 2 and more miRNA*s. (*B*) Analysis of miRNA* profiles by Northern blots. Red arrows indicate the differential bands (corresponding to *A*) caused by ATRM2 mutation. LMW RNA extracted from inflorescence tissues of indicated genotypes was used. U6 was used as a loading control. Note that the same membranes as in Fig. 2 were used.

significantly correlated in *hen1 atrm2* versus *hen1* (Fig. 4 *B* and *C*), which implies that ATRM2 may act on miRNA/miRNA* duplexes. Strikingly, ATRM2 malfunction also changes the profiles of several miRNA*s, with a markedly increased trimming (Fig. 5*A* and *SI Appendix*, Fig. S11*A*). The result was further validated by Northern blot (Fig. 5*B* and *SI Appendix*, Fig. S11*B*). Considering ATRM2 is a 3′ to 5′ exoribonuclease, another yet unknown trimmer(s) must confer miRNA* trimming, either upstream or downstream of ATRM2. We then examined whether increased miRNAs* in *atrm2-1* were bound to AGO1 through AGO1 immunoprecipitation followed by Northern blot or small RNA deep sequencing. However, no overaccumulation of AGO1-bound miRNA*s was detected in *hen1-8 heso1-1 atrm2-1* (*SI Appendix*, Fig. S12), suggesting that ATRM2 may not be involved in miRNA/miRNA* strand selection and/or duplex unwinding.

ATRM2 Colocalizes and Interacts with AGO1. Our in vivo data suggest that ATRM2 may be involved in miRNA/miRNA* degradation but is downstream of HEN1 (Figs. 1*B* and 2). Thus, ATRM2 likely functions in the initiation stage of RISC assembly before duplex unwinding. If this were the case, we would see a physical association between ATRM2 and AGO1. We first transiently expressed ATRM2-GFP under the control of a Cauliflower mosaic virus (CaMV) 35S promoter in *Arabidopsis* protoplast and *Nicotiana benthamiana*. The ATRM2-GFP signal was mainly detected in cytoplasm (Fig. 6 *A* and *C*). We also performed nuclear-cytoplasmic fractionation (36) using a complementation line expressing *pATRM2::ATRM2-GFP*. The quality of nuclear-cytoplasmic fractionation was assessed by Actin and H3, which are markers of cytoplasm and nucleus, respectively. ATRM2-GFP protein was mainly detected in the cytoplasm fraction, similar to AGO1 (Fig. 6*B*) (11, 16, 37). We then checked whether ATRM2 was colocalized with AGO1. We coexpressed ATRM2-GFP and RFP-AGO1 in *N. benthamiana* leaves and found that the RFP-AGO1 signal was partially overlapped with ATRM2-GFP, with RFP-AGO1 more abundant in the nucleus than ATRM2-GFP (Fig. 6*C*). The nuclear localization of AGO1 is consistent with recent findings that RISC assembly occurs in the nucleus and AGO1 can directly interact with chromatin

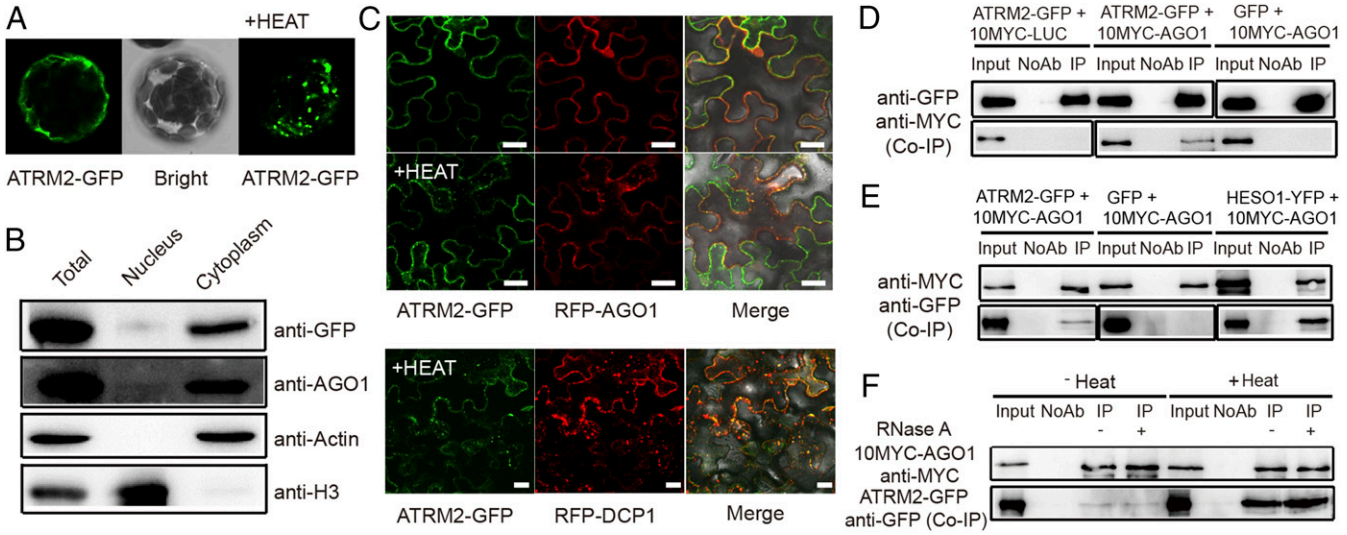

Fig. 6. ATRM2 colocalizes and interacts with AGO1. (*A*) Transiently expressed ATRM2-GFP in *Arabidopsis* protoplast. +Heat, 37 °C for 30 min. (Magnification: 750×.) (*B*) Nuclear-cytoplasmic fractionation assay of ATRM2. Total proteins extracted from *pATRM2::ATRM2-GFP* transgenic plants were used. Actin and Histone 3 (H3) served as cytoplasmic and nucleus markers, respectively. (*C*) Colocalization of ATRM2-GFP and RFP-AGO1/DCP1-RFP in *N. benthamiana* leaves. +Heat, 42 °C for 60 min. (*D*) 10xMYC-AGO1 coimmunoprecipitates with ATRM2-GFP. (*E*) ATRM2-GFP coimmunoprecipitates with 10xMYC-AGO1. (*F*) Heat treatment enhances ATRM2 and AGO1 interaction. +Heat, 42 °C for 60 min. For IP, input = 25%; for Co-IP, input = 0.7%. LUC, Luciferase protein, which served as a negative control; NoAb, no antibody control. (Scale bar: 25 μm.)

to promote gene expression (38, 39). It has been reported that AGO1 enriches in stress granules under heat stress (40). We then tested whether ATRM2 colocalizes with AGO1 in stress granules after heat treatment. Indeed, ATRM2-GFP and RFP-AGO1 are colocalized in discrete cytoplasmic foci after a 1-h 42 °C treatment. In addition, ATRM2-GFP was colocalized with DCP1-RFP, DCP2-RFP, and PABP8-RFP (Fig. 6*C* and *SI Appendix*, Fig. S13), confirming these cytoplasmic foci are bona fide stress granules.

We next investigated whether ATRM2 physically interacts with AGO1. We transiently expressed respective pairs of tagged proteins in *N. benthamiana* and performed coimmunoprecipitation (co-IP) assays. GFP-Trap beads and anti-MYC beads were used to capture GFP-tagged and MYC-tagged proteins, respectively. We were able to detect ATRM2-GFP in the MYC-AGO1 immunoprecipitates and MYC-AGO1 in the ATRM2-GFP immunoprecipitates (Fig. 6 *D* and *E* and *SI Appendix*, Fig. S15 *A* and *B*). As negative controls, 10xMYC-LUC (Luciferase) did not co-IP with ATRM2-GFP and GFP alone did not co-IP with MYC-AGO1, and protein A beads without antibody failed to capture both proteins (Fig. 6 *D* and *E*). The interaction between HESO1-GFP and 10xMYC-AGO1, which served as a positive control, was stronger than that between ATRM2 and AGO1 (Fig. 6*E*). Consistent with the colocalization results, heat treatment could greatly enhance the ATRM2 and AGO1 interaction (Fig. 6*F* and *SI Appendix*, Figs. S14 and S15*C*). As a control, no interaction was observed between PRL1-GFP and 10xMYC-AGO1 regardless of heat treatment or not (*SI Appendix*, Fig. S14). Moreover, RNaseA treatment failed to abolish the ATRM2-AGO1 interaction (Fig. 6*F*), suggesting that ATRM2 interacts with AGO1 in a miRNA-independent manner.

Discussion

Compared with relatively well-established pathways for small RNA biogenesis, much less is understood for their degradation. HEN1 mediated 3′ end 2′-O-methylation provides a key mechanism in protecting various small RNAs in plants and piRNAs in animals against degradation (9). Previously, we and colleagues found that HESO1 and URT1 cooperatively catalyze unmethylated miRNAs uridylation, which initiates their degradation (11–14). In this study, we identified ATRM2, a DEDDy type 3′ to 5′ exoribonuclease (Fig. 1*B*), as another *hen1* suppressor through a reverse genetic approach.

ATRM2 has a profound effect only when HEN1 function is compromised (Figs. 1*B* and 2 and *SI Appendix*, Fig. S5*A*), indicating that ATRM2 targets unmethylated small RNA species and acts downstream of HEN1. ATRM2 is likely not a trimmer because trimming of miRNAs was only marginally affected (Figs. 2 and 3*D* and *SI Appendix*, Fig. S9). In addition, ATRM2 is not specifically involved in the degradation of uridylated miRNAs, as *atrm2* could rescue the phenotype of *hen1-2 heso1-2 urt1-3*, a mutant with almost complete loss of U tailing (Fig. 3) (11). In fact, *atrm2*, but not *heso1*, restored the phyllochron defects of *hen1* (Fig. 1*B*). Moreover, *atrm2* appeared to have a more profound effect when uridylation was impaired (Figs. 2 and 3*D*). One possible explanation for this observation is that accumulated unmethylated miRNAs caused by ATRM2 malfunction can further be degraded through the uridylation-mediated miRNA decay pathway.

Interestingly, we detected a significant coregulation of miRNAs and their corresponding miRNA*s by ATRM2 in the *hen1* background (Fig. 4 *B* and *C*). This implies that ATRM2 may act on miRNA/miRNA* duplexes rather than single stranded miRNAs. Unfortunately, we were unable to detect any robust activities of ATRM2 on single strand miR156, miR156/miR156* duplex, or miRNAs from AGO1 imunoprecipitates. Considering the facts that ATRM2 itself does not contain any dsRBD domain and functions downstream of HEN1, we postulate that ATRM2 may function during RISC loading before duplex unwinding (Fig. 7). Consistent with this model, we found that ATRM2 colocalized and physically interacted with AGO1 (Fig. 6 *C*–*F*). Because AGO distinguishes miRNAs from miRNA*s, this may also help explain why several miRNA*s, but not miRNAs, are trimmed in *atrm2* mutant (Fig. 5 and *SI Appendix*, Fig. S11).

Unlike HESO1, ATRM2 only regulates a limited number of miRNAs in vivo. There are two possible interpretations of this observation: (*i*) ATRM2 is a general factor, while multiple feedback mechanisms exist for the regulation of miRNA steady levels; and (*ii*) ATRM2 may recognize specific motifs or structures

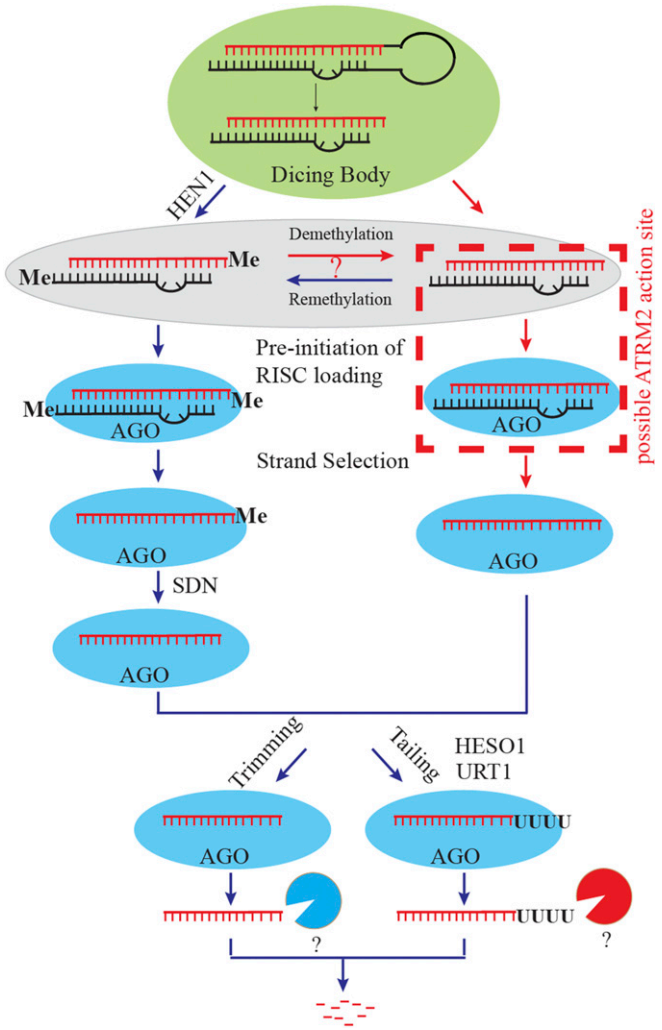

Fig. 7. A proposed working model for ATRM2 function. Gray oval, proposed locations adjacent to AGO proteins, which are physically distinct from miRNA-producing sites (i.e., Dicing bodies). Red dashed square, possible ATRM2 action site. Blue and red major sectors, uncharacterized exoribonucleases for the degradation of trimmed and uridylated miRNAs, respectively.

of miRNA/miRNA* duplex. Nevertheless, our attempts to find such cis-elements were not successful.

Strikingly, we found that miR390, but not all other tested miRNAs and miRNA*s including miR390*, were significantly more methylated in *hen1-8 heso1-1 atrm2-1* than in *hen1-8 heso1-1* (*SI Appendix*, Fig. S6). The mechanism for miR390 remethylation is currently unknown. We guess this phenomenon may be related to the specific association of miR390 with AGO7. To provide specificity, at least part of HEN1-mediated methylation must occur at or very close to each AGO site, positionally different from the nascent small RNA duplex generating loci (e.g., D-body for most miRNA/miRNA*s) (41). Since plant HEN1 specifically recognizes miRNA/miRNA* duplex (4, 42), it seems that increased miR390/miR390* by *ATRM2* mutation is more likely at their unloaded status. We propose two possible mechanisms: (*i*) A specific connection between HEN1 and AGO7 marks this specificity; and (*ii*) HEN1 works nonspecifically at different AGOs. While many small RNAs compete for limited HEN1 activity at other AGO sites, it is reasonable that we did not see an obvious increase of methylation for individual miRNAs. A more accurate examination of methylation is required for testing this hypothesis.

Since a small proportion of miRNAs is unmethylated when HEN1 is fully competent, we envision that ATRM2 behaves the same in WT (11). Indeed, we found that miR158* was more trimmed in *atrm2* compared with that in Col-0 (Fig. 5*A* and *SI Appendix*, Fig. S11*A*), resembling the observations in HEN1 compromised mutants (Fig. 5 and *SI Appendix*, Fig. S11). This is consistent with our sequencing results (*SI Appendix*, Fig. S9*B*) and previous report that miR158 is partially unmethylated in WT background (15). The biological significance of ATRM2 in WT is still unclear. We postulate that ATRM2 may regulate miRNA function in response to abiotic stresses since both ATRM2 and AGO1 were overaccumulated in stress granules after heat treatment. Moreover, ATRM2 may carry out additional function beyond miRNA regulation. In fact, it has been reported that ATRM2 is responsible for the shortening of a set of long siRNAs (28).

Materials and Methods

Plant Materials. All mutants are in the Col-0 ecotype, except *hen1-1*, *hen1-2*, *heso1-2*, *urt1-3*, *atrm2-2*, *atrm2-3*, and their high order mutants, which are in the L*er* ecotype. *atrm2-2* and *atrm2-3* were generated by CRISPR-Cas9 (29). A detailed protocol for CRISPR-Cas9 can be found in *SI Appendix, Supplemental Materials and Methods*.

qPCR Analysis and Small RNA Northern Blotting. qPCR analysis, β-elimination assay, and small RNA Northern blotting were performed as previously described (11, 12). For small RNA Northern blot, either biotin labeled (for *SI Appendix*, Fig. S10) or ^{32}P-labeled probes (for all others) were used.

Small RNA Library Construction and Deep Sequencing. Total RNAs or anti-AGO1 (16) immunoprecipitated small RNAs extracted from inflorescence tissues of each indicated genotypes were used for sRNA library construction. The deep-sequencing data were deposited to Gene Expression Omnibus (GEO) database (https://www.ncbi.nlm.nih.gov/geo/) under accession no. GSE107070. A detailed protocol for sequencing data analysis can be found in *SI Appendix, Supplemental Materials and Methods*.

Coimmunoprecipitation. pGWB521-AGO1 (*p35S:10xMYC-AGO1*), pEarleyGate 101-HESO1 (*p35S::HESO1-YFP*), and pMDC83-PRL1 (*p35S::PRL1-GFP*) were previously described (11, 43). pGWB521-LUC (*p35S:10xMYC-LUC*) was generated in the same way and used as a negative control. *p35S::*ATRM2-GFP and 10xMYC-tagged AGO1 were coexpressed in the presence of P19 in *N. benthamiana* leaves for 72 h and harvested. Protein extraction and coimmunoprecipitation analysis were performed as previously described (44). GFP-Trap beads (gta-20, ChromoTek) and anti-MYC (A7470, Sigma) agarose beads were used to immunoprecipitate the GFP-tagged and 10xMYC-tagged proteins, respectively. Anti-MYC (AM1007a, Abgent) and anti-GFP (MMS-118R, Covance) were diluted at 1:2,500 and used for the Western blot assay.

Nuclear-Cytoplasmic Fractionation Assay. Nuclear-cytoplasmic fractionation assay was performed according to a previous description (36). Inflorescence tissues from *hen1-8 heso1-1 atrm2-1* + *pATRM2::ATRM2-GFP* transgenic plants were used as starting materials. Anti-H3 (AS10710, Agrisera), anti-Actin2 (60008–1-Ig, Proteintech), anti-AGO1, and anti-GFP were diluted at 1:2,500 and used for the Western blot assay.

Exoribonuclease BLAST, Genomic Complementation, and Confocal Microscopy. Methods for exoribonuclease BLAST, genomic complementation, and confocal microscopy are described in *SI Appendix, Supplemental Materials and Methods*.

DNA and RNA Oligos. All primers and oligos for genotyping, qPCR, plasmid construction, and Northern blots used in this study are listed in Dataset S4.

ACKNOWLEDGMENTS. We thank Dr. Donald P. Weeks for the CRISPR-Cas9 cloning vector, Dr. Shuxin Zhang for the *p35S*::PRL1-GFP plasmid, and Dr. Xiao Zhou for critical reading of the manuscript. This work was supported by grants from the National Key R&D Program of China (2016YFA0503200), the National Natural Science Foundation of China (31622009, 91740101, and 31771480), and the China Postdoctoral Science Foundation (2015M581522).

1. Rogers K, Chen X (2013) Biogenesis, turnover, and mode of action of plant microRNAs. *Plant Cell* 25:2383–2399.
2. Park W, Li J, Song R, Messing J, Chen X (2002) CARPEL FACTORY, a Dicer homolog, and HEN1, a novel protein, act in microRNA metabolism in Arabidopsis thaliana. *Curr Biol* 12:1484–1495.
3. Xie Z, et al. (2005) Expression of Arabidopsis MIRNA genes. *Plant Physiol* 138: 2145–2154.
4. Yu B, et al. (2005) Methylation as a crucial step in plant microRNA biogenesis. *Science* 307:932–935.
5. Fang X, Qi Y (2016) RNAi in plants: An Argonaute-centered view. *Plant Cell* 28: 272–285.
6. Iki T (2017) Messages on small RNA duplexes in plants. *J Plant Res* 130:7–16.
7. Kobayashi H, Tomari Y (2016) RISC assembly: Coordination between small RNAs and Argonaute proteins. *Biochim Biophys Acta* 1859:71–81.
8. Eamens AL, Smith NA, Curtin SJ, Wang MB, Waterhouse PM (2009) The Arabidopsis thaliana double-stranded RNA binding protein DRB1 directs guide strand selection from microRNA duplexes. *RNA* 15:2219–2235.
9. Ren G, Chen X, Yu B (2014) Small RNAs meet their targets: When methylation defends miRNAs from uridylation. *RNA Biol* 11:1099–1104.
10. Li J, Yang Z, Yu B, Liu J, Chen X (2005) Methylation protects miRNAs and siRNAs from a 3′-end uridylation activity in Arabidopsis. *Curr Biol* 15:1501–1507.
11. Wang X, et al. (2015) Synergistic and independent actions of multiple terminal nucleotidyl transferases in the 3′ tailing of small RNAs in Arabidopsis. *PLoS Genet* 11: e1005091.
12. Ren G, Chen X, Yu B (2012) Uridylation of miRNAs by hen1 suppressor1 in Arabidopsis. *Curr Biol* 22:695–700.
13. Zhao Y, et al. (2012) The Arabidopsis nucleotidyl transferase HESO1 uridylates unmethylated small RNAs to trigger their degradation. *Curr Biol* 22:689–694.
14. Tu B, et al. (2015) Distinct and cooperative activities of HESO1 and URT1 nucleotidyl transferases in microRNA turnover in Arabidopsis. *PLoS Genet* 11:e1005119.
15. Zhai J, et al. (2013) Plant microRNAs display differential 3′ truncation and tailing modifications that are ARGONAUTE1 dependent and conserved across species. *Plant Cell* 25:2417–2428.
16. Ren G, et al. (2014) Methylation protects microRNAs from an AGO1-associated activity that uridylates 5′ RNA fragments generated by AGO1 cleavage. *Proc Natl Acad Sci USA* 111:6365–6370.
17. Zuo Y, Deutscher MP (2001) Exoribonuclease superfamilies: Structural analysis and phylogenetic distribution. *Nucleic Acids Res* 29:1017–1026.
18. Maiti M, Lee HC, Liu Y (2007) QIP, a putative exonuclease, interacts with the Neurospora Argonaute protein and facilitates conversion of duplex siRNA into single strands. *Genes Dev* 21:590–600.
19. Han BW, Hung JH, Weng Z, Zamore PD, Ameres SL (2011) The 3′-to-5′ exoribonuclease Nibbler shapes the 3′ ends of microRNAs bound to Drosophila Argonaute1. *Curr Biol* 21:1878–1887.
20. Liu N, et al. (2011) The exoribonuclease Nibbler controls 3′ end processing of microRNAs in Drosophila. *Curr Biol* 21:1888–1893.
21. Czech B, Hannon GJ (2016) A happy 3′ ending to the piRNA maturation story. *Cell* 164: 838–840.
22. Tops BB, et al. (2005) RDE-2 interacts with MUT-7 to mediate RNA interference in Caenorhabditis elegans. *Nucleic Acids Res* 33:347–355.
23. Hayashi R, et al. (2016) Genetic and mechanistic diversity of piRNA 3′-end formation. *Nature* 539:588–592.
24. Ramachandran V, Chen X (2008) Degradation of microRNAs by a family of exoribonucleases in Arabidopsis. *Science* 321:1490–1492.
25. Yu Y, et al. (2017) ARGONAUTE10 promotes the degradation of miR165/6 through the SDN1 and SDN2 exonucleases in Arabidopsis. *PLoS Biol* 15:e2001272.
26. Sanei M, Chen X (2015) Mechanisms of microRNA turnover. *Curr Opin Plant Biol* 27: 199–206.
27. Glazov E, et al. (2003) A gene encoding an RNase D exonuclease-like protein is required for post-transcriptional silencing in Arabidopsis. *Plant J* 35:342–349.
28. Ye R, et al. (2016) A Dicer-independent route for biogenesis of siRNAs that direct DNA methylation in Arabidopsis. *Mol Cell* 61:222–235.
29. Jiang W, et al. (2013) Demonstration of CRISPR/Cas9/sgRNA-mediated targeted gene modification in Arabidopsis, tobacco, sorghum and rice. *Nucleic Acids Res* 41:e188.
30. Wu G, et al. (2009) The sequential action of miR156 and miR172 regulates developmental timing in Arabidopsis. *Cell* 138:750–759.
31. Hunter C, Sun H, Poethig RS (2003) The Arabidopsis heterochronic gene ZIPPY is an ARGONAUTE family member. *Curr Biol* 13:1734–1739.
32. Wang JW, Czech B, Weigel D (2009) miR156-regulated SPL transcription factors define an endogenous flowering pathway in Arabidopsis thaliana. *Cell* 138:738–749.
33. Montgomery TA, et al. (2008) Specificity of ARGONAUTE7-miR390 interaction and dual functionality in TAS3 trans-acting siRNA formation. *Cell* 133:128–141.
34. Nakano M, et al. (2006) Plant MPSS databases: Signature-based transcriptional resources for analyses of mRNA and small RNA. *Nucleic Acids Res* 34:D731–D735.
35. Kozomara A, Griffiths-Jones S (2014) miRBase: Annotating high confidence microRNAs using deep sequencing data. *Nucleic Acids Res* 42:D68–D73.
36. Wang W, et al. (2011) An importin β protein negatively regulates microRNA activity in Arabidopsis. *Plant Cell* 23:3565–3576.
37. Zhang Z, et al. (2017) KETCH1 imports HYL1 to nucleus for miRNA biogenesis in *Arabidopsis*. *Proc Natl Acad Sci USA* 114:4011–4016.
38. Bologna NG, et al. (2018) Nucleo-cytosolic shuttling of ARGONAUTE1 prompts a revised model of the plant microRNA pathway. *Mol Cell* 69:709–719.e5.
39. Liu C, et al. (2018) Arabidopsis ARGONAUTE 1 binds chromatin to promote gene transcription in response to hormones and stresses. *Dev Cell* 44:348–361.e7.
40. Pomeranz MC, et al. (2010) The Arabidopsis tandem zinc finger protein AtTZF1 traffics between the nucleus and cytoplasmic foci and binds both DNA and RNA. *Plant Physiol* 152:151–165.
41. Fang Y, Spector DL (2007) Identification of nuclear dicing bodies containing proteins for microRNA biogenesis in living Arabidopsis plants. *Curr Biol* 17:818–823.
42. Huang Y, et al. (2009) Structural insights into mechanisms of the small RNA methyltransferase HEN1. *Nature* 461:823–827.
43. Zhang S, Liu Y, Yu B (2014) PRL1, an RNA-binding protein, positively regulates the accumulation of miRNAs and siRNAs in Arabidopsis. *PLoS Genet* 10:e1004841.
44. Ren G, et al. (2012) Regulation of miRNA abundance by RNA binding protein TOUGH in Arabidopsis. *Proc Natl Acad Sci USA* 109:12817–12821.